ATLAS NOTE : ATL-LARG-98-109

EDMS # : ATL-AB-EN-0009

November 98

ELECTRICAL TESTS OF E.M. BARREL PRESAMPLER SECTORS

Abstract

A description of the tests and electronics used to control the presampler sectors, before and after their assembly, is given. An example of the results obtained for the first two sectors, tested at room and liquid nitrogen temperatures, is shown.

B. Belhorma, J.Y. Hostachy,

D. Dzahini, J. Collot

ISN - IN2P3 - CNRS

Université Joseph Fourier, Grenoble, France

1 Introduction

The barrel presampler is composed of 512 modules of 8 different types, assembled in 64 sectors. In order to avoid problems at the last moment, modules, mother-boards and cable solderings are tested separately before assembly. Some of these tests are performed at both room and liquid nitrogen temperatures. Then, after the validation of each element, the sector is mounted and subsequently controlled by means of a dedicated test bench. The different operations and the test bench will be described in detail in this note.

2 Tests of modules

A series of tests are performed on the modules just after their production and before being equipped with their corresponding mother-boards.

2.1 Insulation tests

The resistances between :
1) the high voltage (HV) buses and the ground (fig. 1),
2) the HV buses and the signal outputs (fig. 2),
3) the signal outputs and the ground (fig. 3)
are measured in air at 1 kV using a high resistance meter. The validation of these tests requires a value larger than 10, 10 and 1 GΩ, respectively.

2.2 Electrode connections

Resistor solderings on anodes, conductive strip lines in electrodes, etc... are checked by injecting a low amplitude (10 V peak-to-peak) and a low frequency (2 kHz) sinusoidal signal into each high voltage line, separatly, and by measuring the average amplitude of the response at each signal output using a digital oscilloscope (fig. 4). The response is a sinusoidal signal the amplitude of which depends on the number N of anodes per detection cell as shown in table 1.

A simulation using Spice software has been performed. The electrical equivalent scheme used for one elementary cell is given on figure 5. The anode is represented by two 300 pF capacitors (C) with the signal output in-between (internal layer of the anode) and C_d is the equivalent capacity of the detection medium between each anode and its neighbouring cathodes (C_d = 8 pF). Figure 6 gives the scheme of one detection cell (one channel) in which the number of anodes (N) depends on the module type (see table 1). Finally, the scheme of one module is given on figure 7. The simulation shows that a 1 MΩ protection resistor not being properly soldered would result in an amplitude decrease of 1/2N in the corresponding channel, i.e., approximately 20 mV which can be easily observed with the numerical oscilloscope.

Table 1: Response to a sinusoidal signal for the 8 types of modules

Module type	Number of anodes/channel	Amplitude (mV) at room temperature	Amplitude (mV) at 77 $^\circ K$
1	7	281	210
2	8	318	246
3	9	358	280
4	10	398	312
5	11	438	350
6	13	512	420
7	16	624	518
8	18	680	600
	14	542	476

3 Test of mothers boards

Mechanical and electrical tests are performed on the MBs upon reception. The dimensions of each type of MB are checked at room temperature, with a tolerance of ± 0.1 mm. Then, the flatness is controlled by applying a 2N weight at the center of each MB; the resulting values must be within ± 1 mm. The linear contraction coefficient is also measured by immersing the MBs in liquid nitrogen. This coefficient must be equal to $(0.25 \pm 0.05)\%$. After warming up the MBs, the conduction of all internal strips is checked.

After validation of all these tests, MBs are sent to another company to be cabled. The schematic diagram of the calibration system is shown on figure 9 for MBs of types 1 to 7, and figure 10 for MBs of type 8. Upon reception again, a visual inspection is performed on the MBs. Then the solderings of the surface mounted resistors (0.1 % accuracy) are checked by measuring the resistance between the calibration and the signal pads with an ohm-meter (fig. 8). For example, with the mother board of type # 3, this measured resistance is equal to $2070 \pm 3\ \Omega$. However :
1- if the 44 Ω main resistor is not connected, (fig. 9), one obtains an infinite value for the resistance in all channels,
2- if one of the 44 Ω dividing resistors is not connected, the resistance read out for the corresponding channel is $2101 \pm 3\ \Omega$,
3- if one of the 51 Ω adaptation resistors is not connected, the resistance read out for the corresponding channel is $2089 \pm 3\ \Omega$,
4- finally, if one of the 2 kΩ injection resistors is not connected, one obtains an infinite value in the corresponding channel.
Thus, any solder default in the calibration system can be easily detected through this measurement, and subsequently corrected.

Table 2: response amplitudes of the modules equipped with their M.Bs.

Module type	Number of anodes per channel	Measured amplitude(mV)	Simulated amplitude (mV)
1	7	270	264
2	8	310	302
3	9	342	334
4	10	385	381
5	11	418	412
6	13	495	482
7	16	605	602
8	18	673	686
	14	528	543

4 Test of the modules equipped with their mother-boards

In order to check simultaneously the solderings between a module and its corresponding mother-board (MB), a low amplitude (10 V peak-to-peak) and low frequency (2 kHz) sinusoidal signal is injected into each HV bus, one after the other. The measured and the simulated output signal amplitudes are given in table 2.

A bad soldering between a module and its MB would mean a null amplitude, and if a 1 MΩ protection resistor is not connected on one anode, then the amplitude will decrease by a factor of 1/N in the corresponding channel; this decrease is twice as large as the value obtained in the case of the module without its MB (see section 2.2).

5 Test of signal cable soldering

Each presampler sector requires two harnesses of coaxial cables. The soldering of the 64 cables in each harness is controlled by using a special box with a system of LEDs labelled from 1 to 64 (according to the cable number). Since the LEDs are set in regular rows, it is easy to check that the LED corresponding to the cable being soldered is lit, when applying on the switch (fig. 11). Because of the micro-dot connector design, where all the cable shielding braids are connected together, it is possible to check only the central wire connection of each coaxial cable.

6 The test bench

A test bench has been built in order to check directly a full azimuthal sector composed of 8 modules. This test bench sits inside a clean room and is composed of a double grid

Faraday cage (4m x 2m x 2.5m) in which there is a liquid nitrogen cryostat (more than 3m long) large enough to contain a presampler sector (fig. 12). Figure 14 shows the test bench electronic setup. The 122 amplifiers and the adjustable time constant shaper allow to simulate the electronics which will be used in the ATLAS detector. All instrument operations (injection, channel selection ...), via GPIB or RS232 connections, are controlled by a PC using a LabWindow application. Signals are first read out by a digital oscilloscope. Results are transmitted to the PC which can complete the analysis. One of the aims of the test bench is to measure the equivalent noise current (ENI) of each channel. Unfortunately the PC behaves like a noise generator at this level of precision. Therefore part of the instruments (amplifiers, multiplexer, shaper) are kept inside the Faraday cage, whereas the PC, the oscilloscope, the generator and the demultiplexer have to be kept outside (fig. 13). The communication between the PC and the multiplexer is performed via opto-electronic links (fig. 15).

The purpose of the test bench is :

- **to check each module at high voltages**. The LeCroy 1451 HV power supply allows to read out the leak current with an accuracy of 10 nA. The result of this operation is automatically transmitted to the PC.

- **to study and calibrate the response of each channel when pulsing test signals through the calibration system**. This test allows to check all electrical mother board connections, calibration and output cables.

- **to measure the noise coming from the 122 channels**. Such a test is very sensitive to a bad ground connection.

- **to check the electrical module connections (electrodes, etc...) when connecting the HV inputs to a low voltage and low frequency sinusoidal signal**. This technique is close to the one described in section 2.2, but in addition each preamplifier gain is first calibrated by injecting another sinusoidal signal with the same frequency into the calibration system. In this case output signals are measured without shaping.

These tests have been performed on 2 sectors at room and at liquid nitrogen temperatures. Data are recorded and then analysed in details with PAW. Figure 16 gives the response waveform when injecting a triangular test pulse into the calibration system. The $CR-RC^2$ shaping time was chosen to be equal to 25 ns, and so close to the value which will be effectively used in the ATLAS detector when applying optimal filtering. The measured response amplitudes V_{cal} of one module and the dispersion around the mean value are shown on figure 17. Noise measurements are then performed to determine the equivalent noise current (ENI). The ENI is the current triangle giving a response amplitude equal to the rms noise voltage σ at the output of the system :

$$ENI = \frac{I_{cal} * \sigma}{V_{cal}}$$

Table 3: Delay between the responses of one sector modules

Module	Measured delay (ns) at room temperature	Expected delay (ns) at LN_2 temperature
1	0	0
2	-1.5	-1.34
3	-2.8	-2.78
4	-3.5	-4.19
5	-4.8	-5.79
6	-6.8	-6.93
7	-6.9	-8.58
8	-8.9	-10.83

σ is obtained by the quadratic difference of the noises measured with the preamplifiers switched on and off, respectively. According to the bandwidth of the shaper [24.5 kHz, 102 MHz], the noise measurements are made every 40 ns during a total time of 2 ms. I_{cal} is the current produced, in each detection cell, by injecting the test pulses into the calibration system. Its value at room temperature is approximately given by $I_{cal} = \frac{V_{triangle}}{33.10^3\ \Omega}$. The distribution of the ENI and its dispersion around the mean value for one module are shown on figure 18. Figure 19 gives the calibrated peak-to-peak amplitude response and its dispersion around the mean value when a sinusoidal signal of 4 V peak-to-peak amplitude and 10 kHz is injected into one of the HV buses. The simulations performed with Spice show that if a single protection resistor is not soldered on some anode, then the ratio will decrease by about 1/N in the corresponding channel. One can see that the accuracy of our measurements is largely better than this value, and allows therefore to check all anode resistors.

7 Delay measurements :

Due to the positions of the modules and the consequently different signal and injection cable lengths, the module responses are delayed with respect to each other. The calculated and the measured delays between the calibration responses of modules within a sector are given in table 3. Module 1 has been taken as a reference.

8 Results of the final electrical tests performed on two presampler sectors

These tests have been performed at room and liquid nitrogen temperatures. Since the presampler sectors will be working at liquid argon temperature in the ATLAS detector, only the results at low temperature are reported here.

Table 4: Leak current of the sectors 01 and 02, at 2 kV, in liquid nitrogen.

HV channel	Leak current (nA) for sector 01	Leak current (nA) for sector 02
1	0	10
2	0	0
3	0	10
4	0	10
5	10	20
6	30	20
7	0	10
8	40	40

8.1 Insulation tests

The results of the high voltage tests performed at 2 kV are given on table 4. The leak current, in each HV channel[1], does not exceed 40 nA with a precision of $\pm$ 10 nA. Same tests conducted on the same sectors in november 98 in liquid argon at CERN for two weeks, yielded to comparable results with no electrode failure detected (0/1356 anodes).

8.2 Calibration tests

Figures 20 and 21 give the response amplitude when triangular signals are injected into the calibration system. The slow slope (channel 1 to 112) is due to the capacity increase of the detection cells implying a larger ballistic deficit. The dispersion around the mean value $\frac{(A - \overline{A}_{module})}{\overline{A}_{module}}$ calculated module per module, is also drawn for each sector. The root mean square of the dispersion is less than 1%, and is essentially due to the fact that there is one amplifier per channel.

8.3 Noise measurements

The equivalent noise current has been measured for both sectors at LN_2 temperature. As shown on figures 22 and 23, the ENI increases with the number of anodes (i.e., according to the detection cell capacities). Its value does not exceed 40 nA and is in good agreement with what was expected. The precision of the ENI measurement : $\sigma(\frac{ENI-\overline{ENI}_{module}}{\overline{ENI}_{module}})$ is about 1% for each module, showing that ground connections are correct.

[1] For more details about the HV distribution into the sector modules, see specification book for the mother boards and the cabling of the e.m. barrel presampler, ATL-AL-ISN-ES-8.0

8.4 Connection tests

Figures 24 and 25 summarize the results of the connection tests (see section 6). As in the previous analysis, the dispersion $\frac{(A - \overline{A}_{module})}{\overline{A}_{module}}$ is calculated taking the mean value of each module separately. The root mean square of these distributions is about 0.5% and therefore one can conclude that all the 1 MΩ resistors are correctly soldered on the anodes.

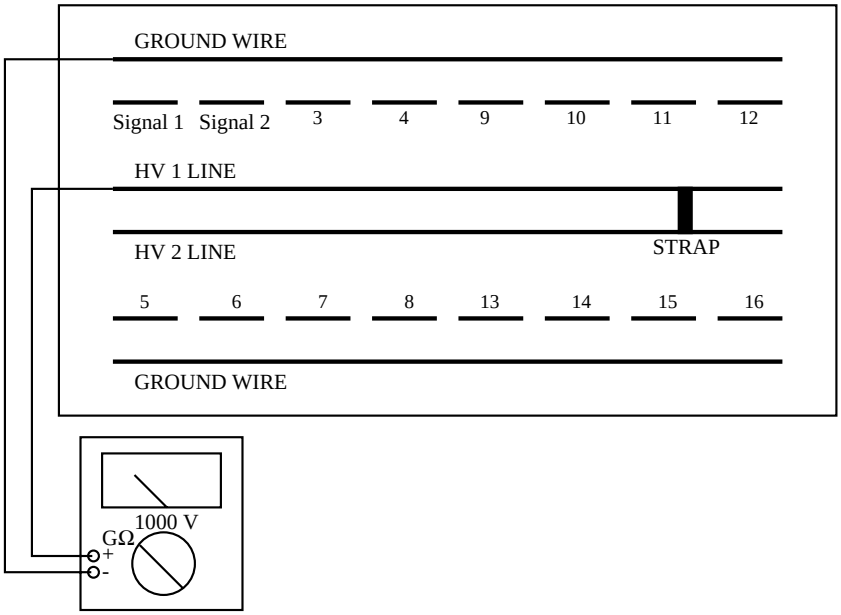

Figure 1: Setup for test # 1.

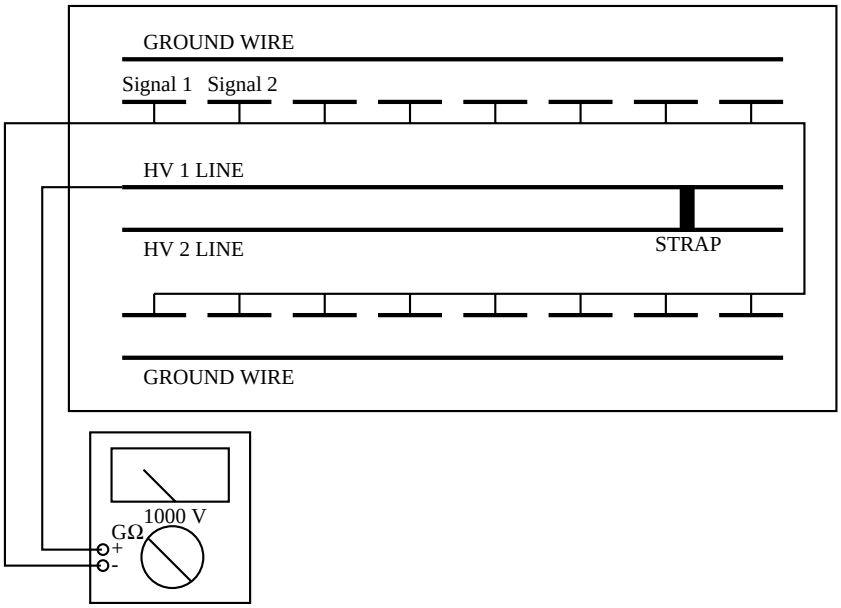

Figure 2: Setup for test # 2.

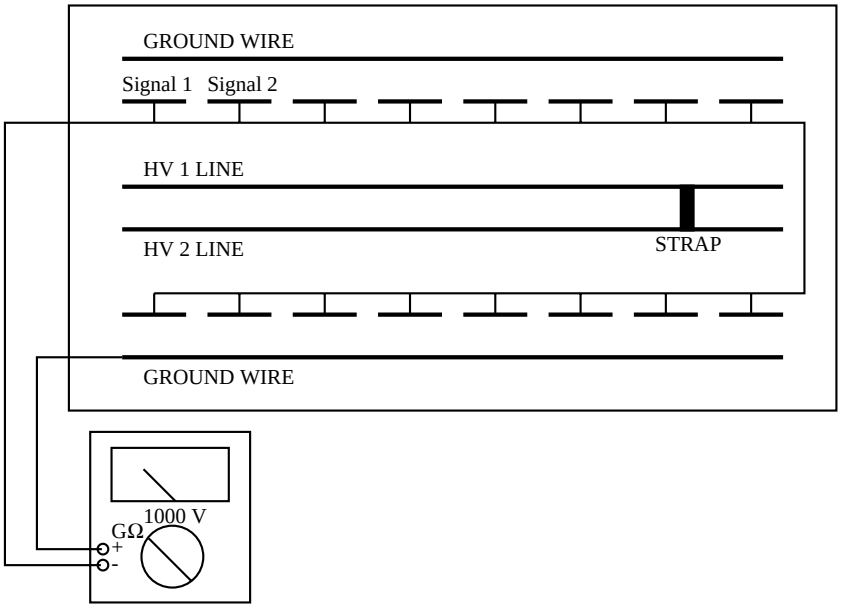

Figure 3: Setup for test # 3.

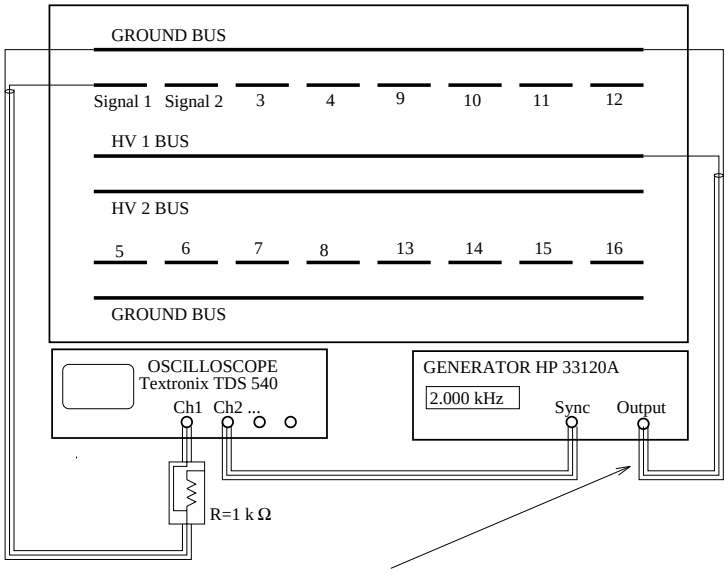

Low amplitude (10V peak to peak) and low frequency sinusoidal signal.

Figure 4: Setup for test # 4.

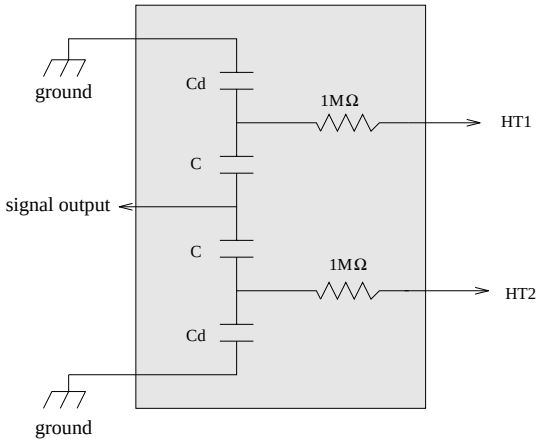

Figure 5: Equivalent electrical scheme of one elementary cell.

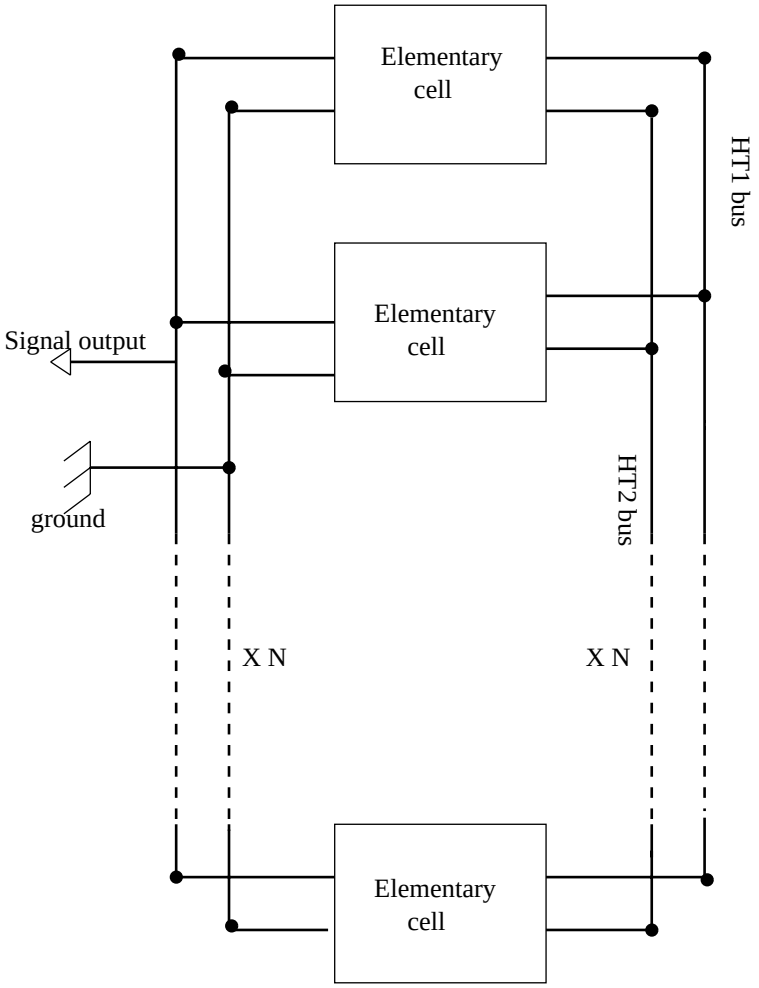

Figure 6: Equivalent electrical scheme of one detection cell (i.e., corresponding to one channel).

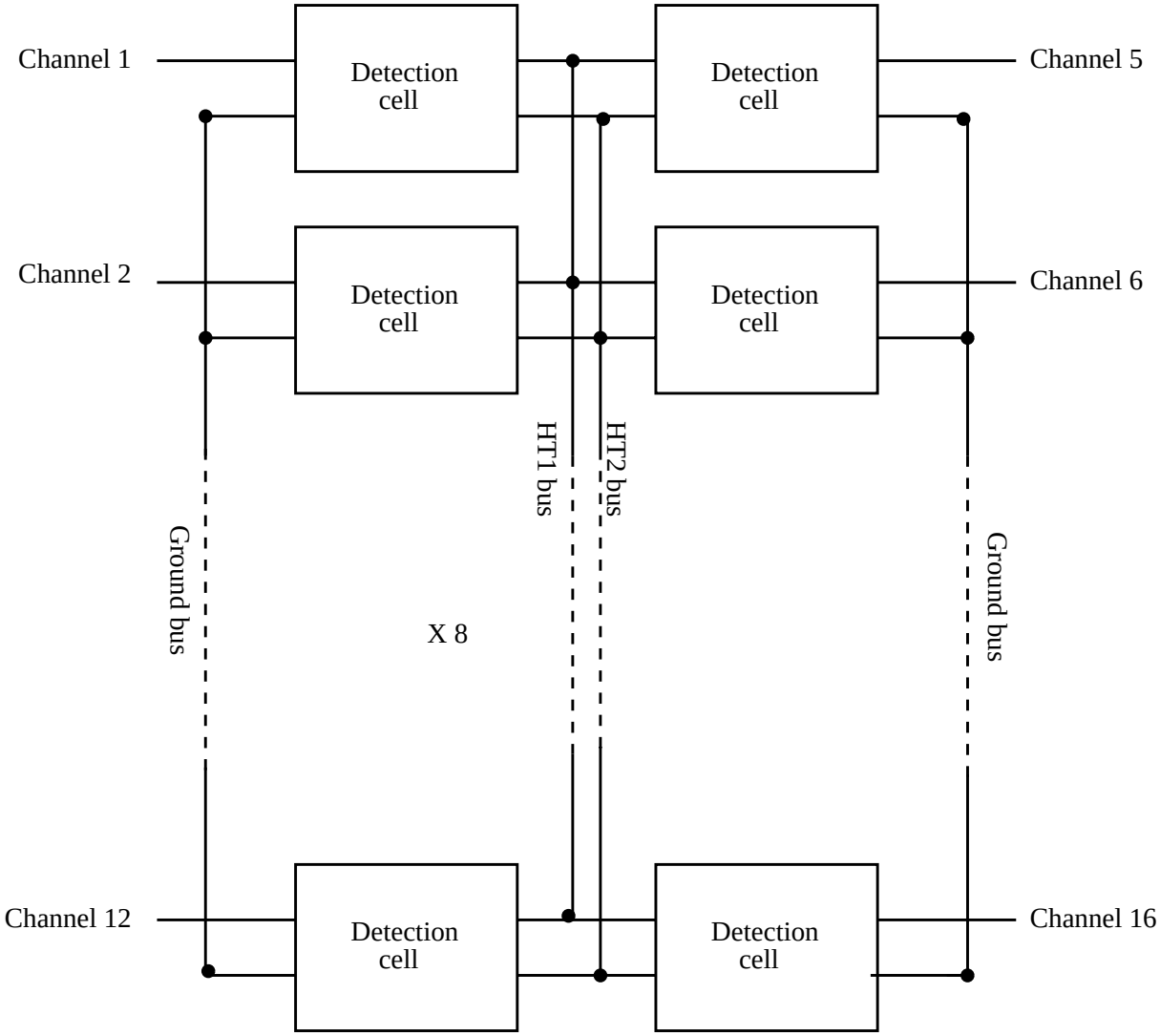

Figure 7: Equivalent electrical scheme of one module (types 1 to 7).

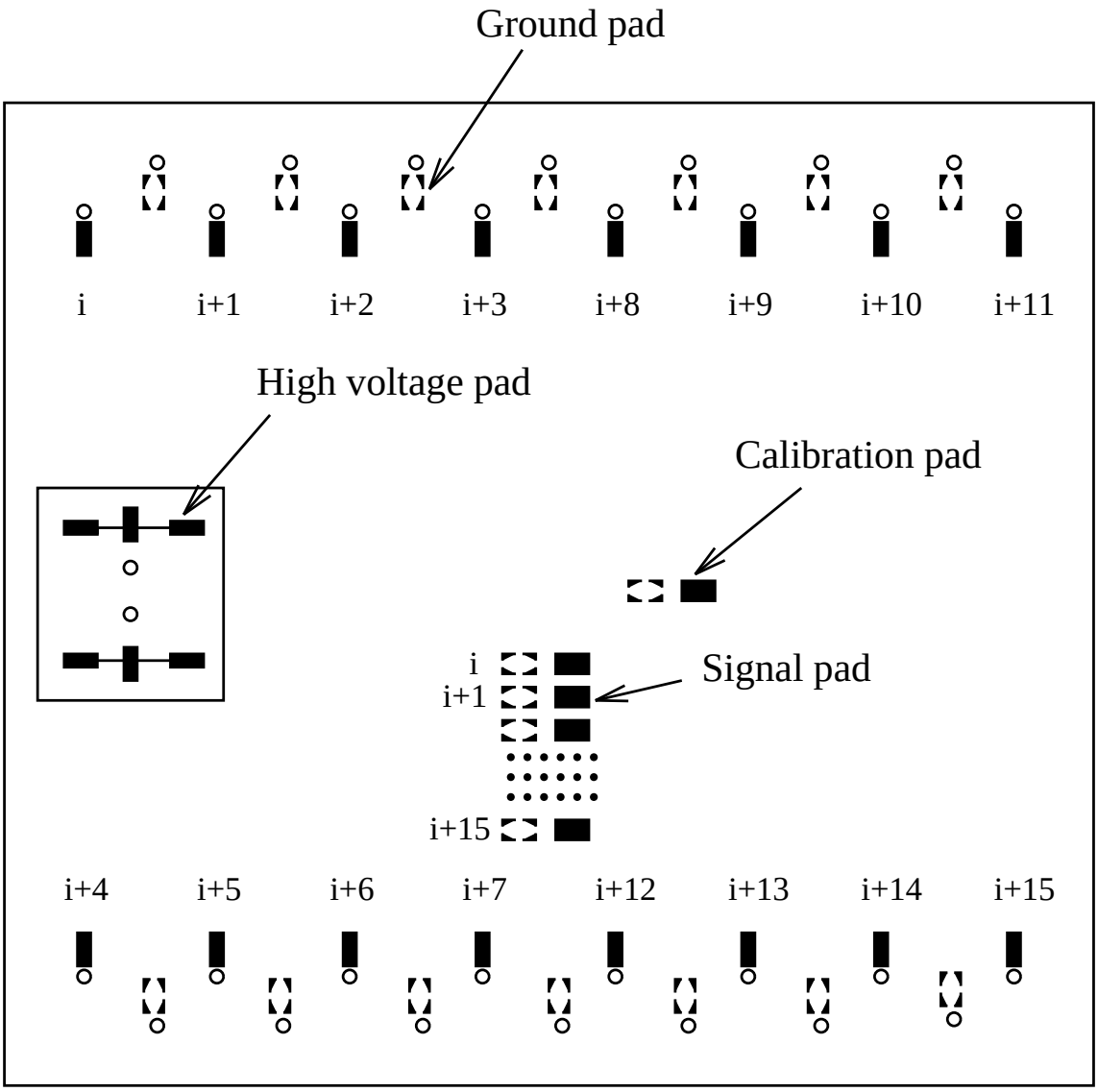

Figure 8: Schematic diagram of a mother board (type 1 to 7).

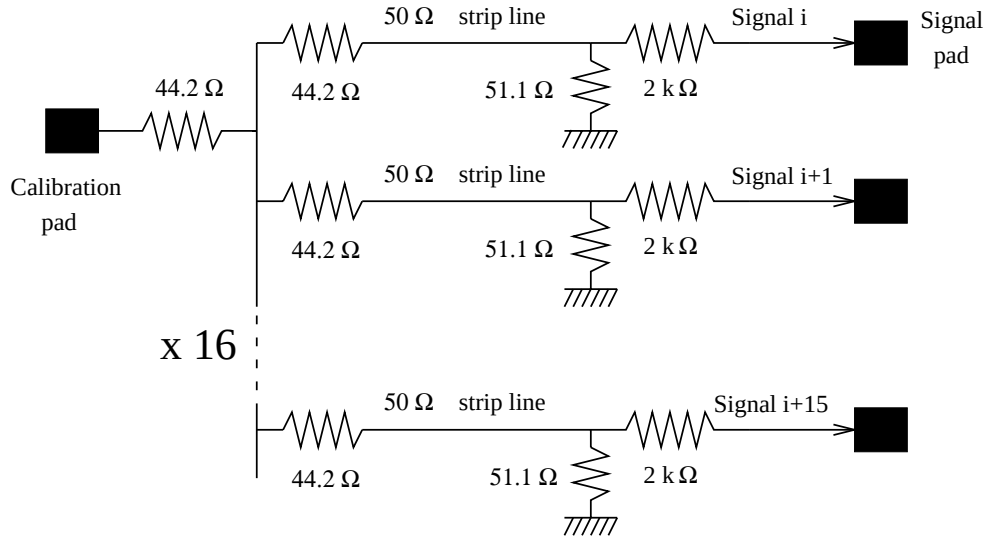

Figure 9: Schematic diagram of the test pulse injection system (MBs 1 to 7).

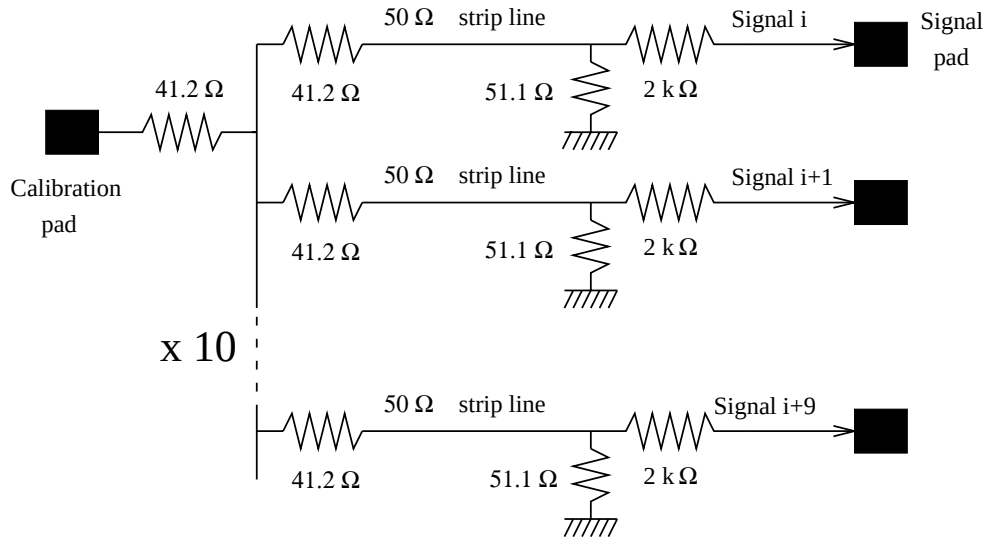

Figure 10: Schematic diagram of the test pulse injection system (MB 8).

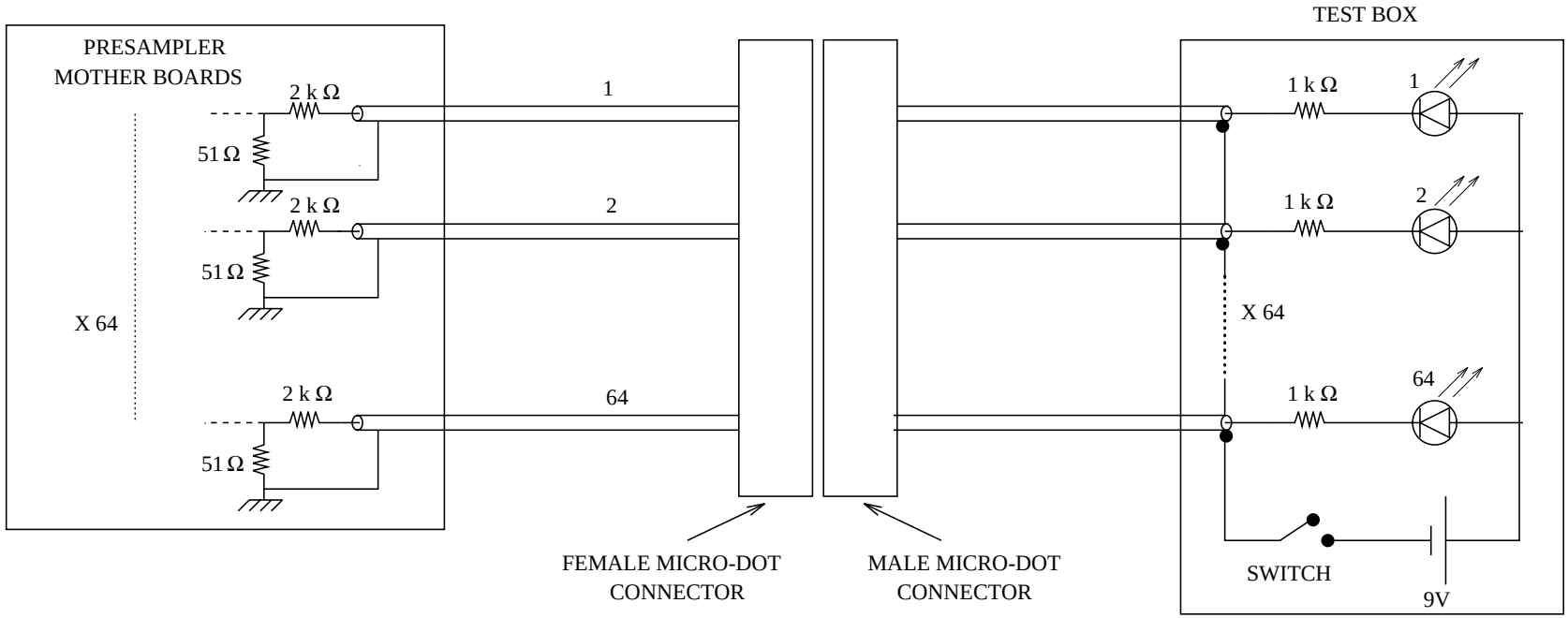

Figure 11: Schematic diagram of the test box with the cable connections.

Figure 12: Photograph of the test bench.

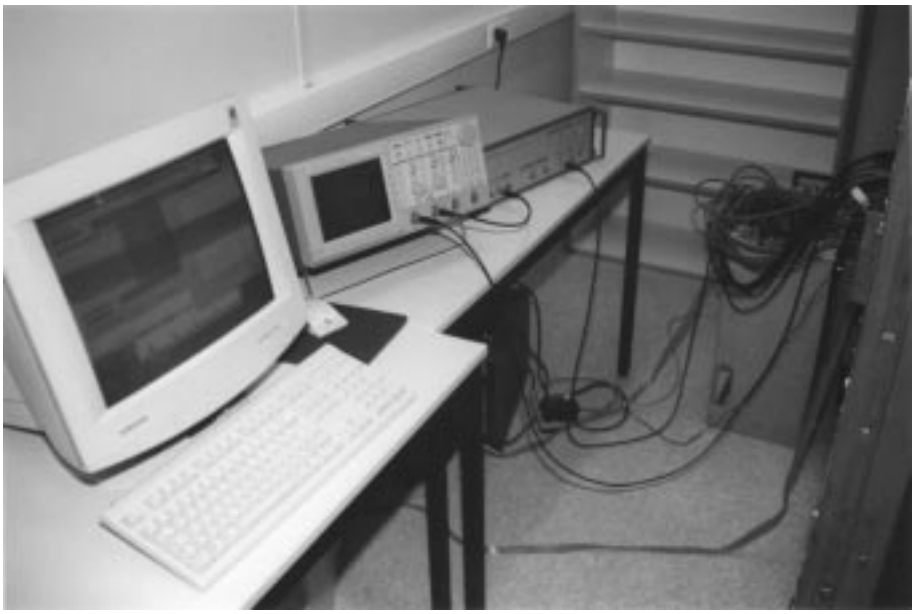

Figure 13: Instruments placed outside the Faraday cage.

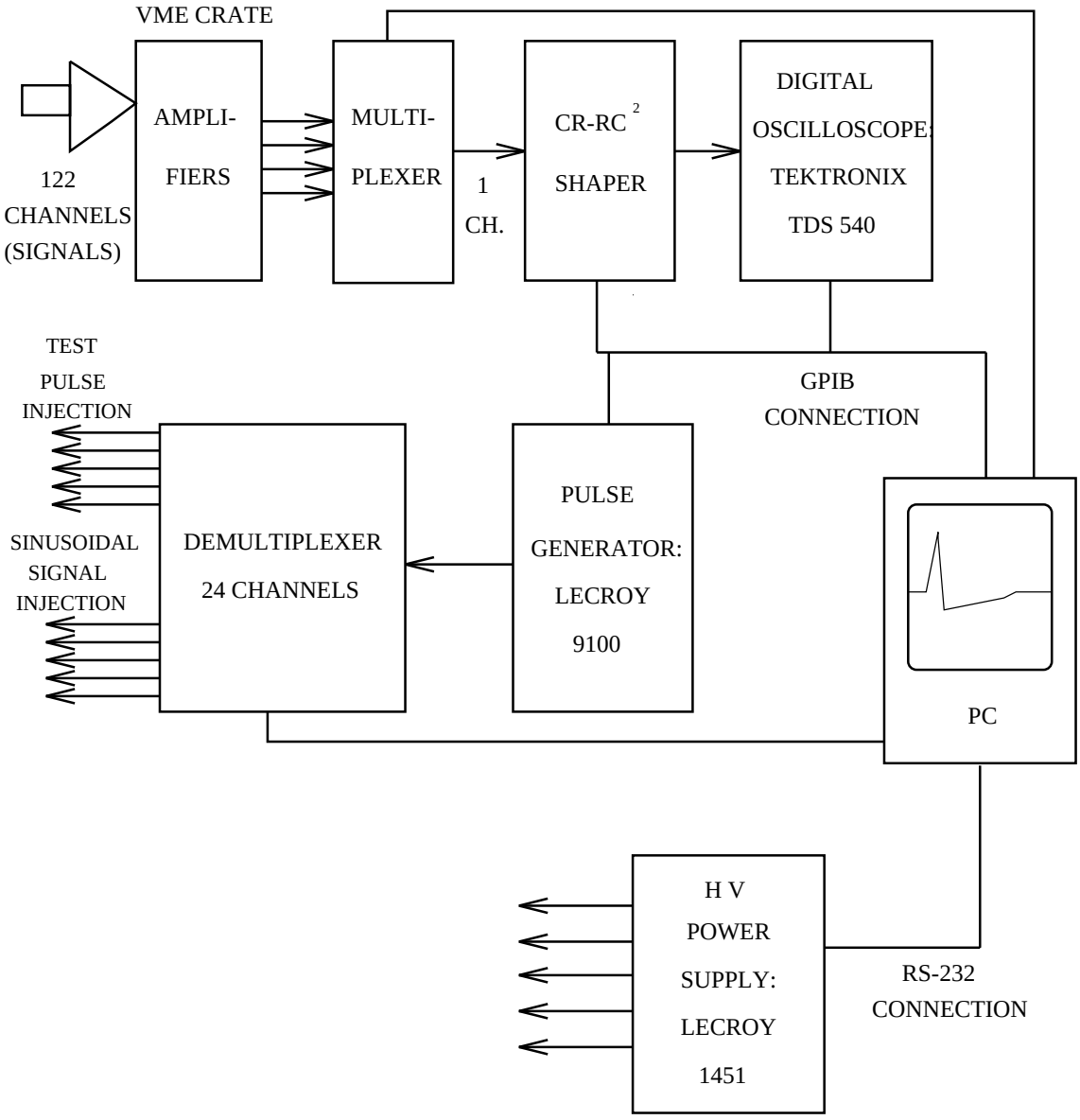

Figure 14: Test bench electronic setup.

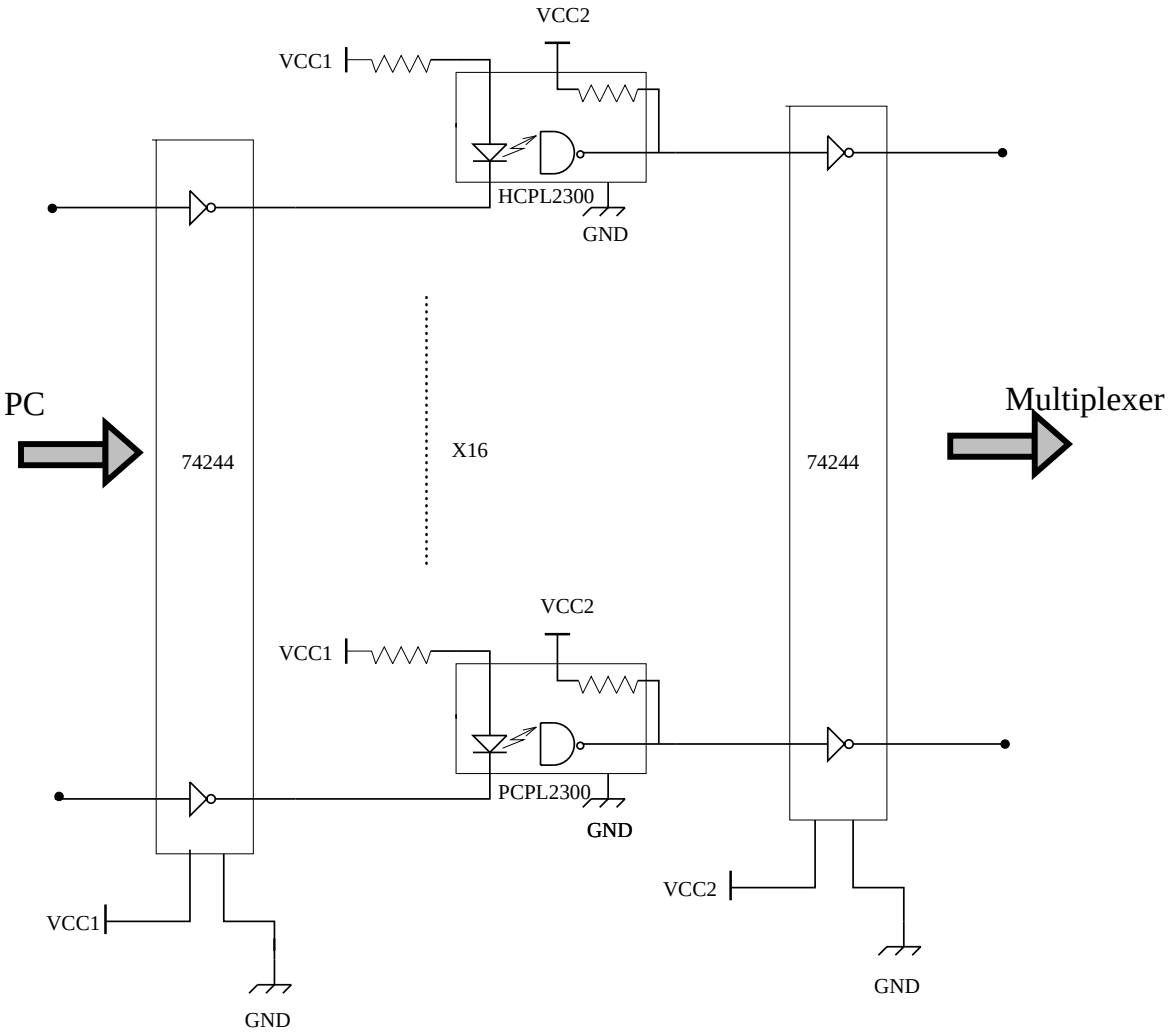

Figure 15: Schematic representation of the opto-electronic link.

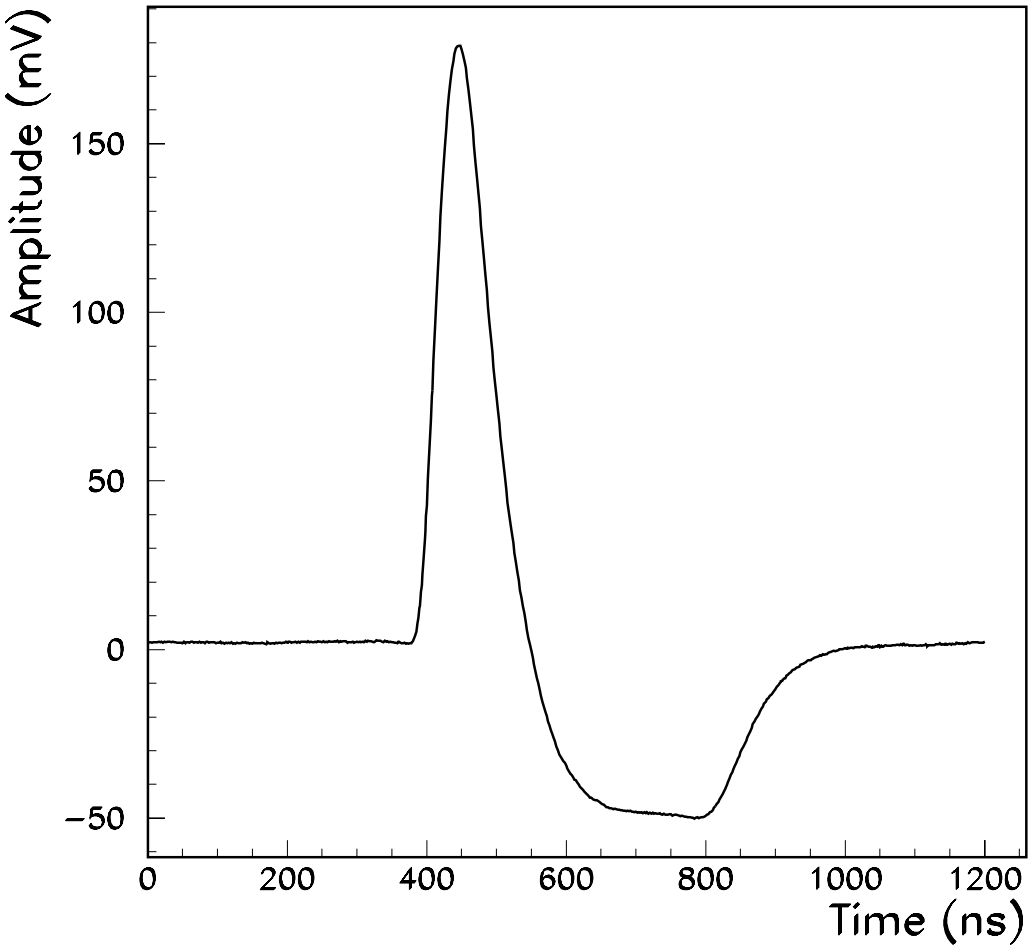

Figure 16: Average response measured at 77 K when injecting triangular pulses into the calibration system.

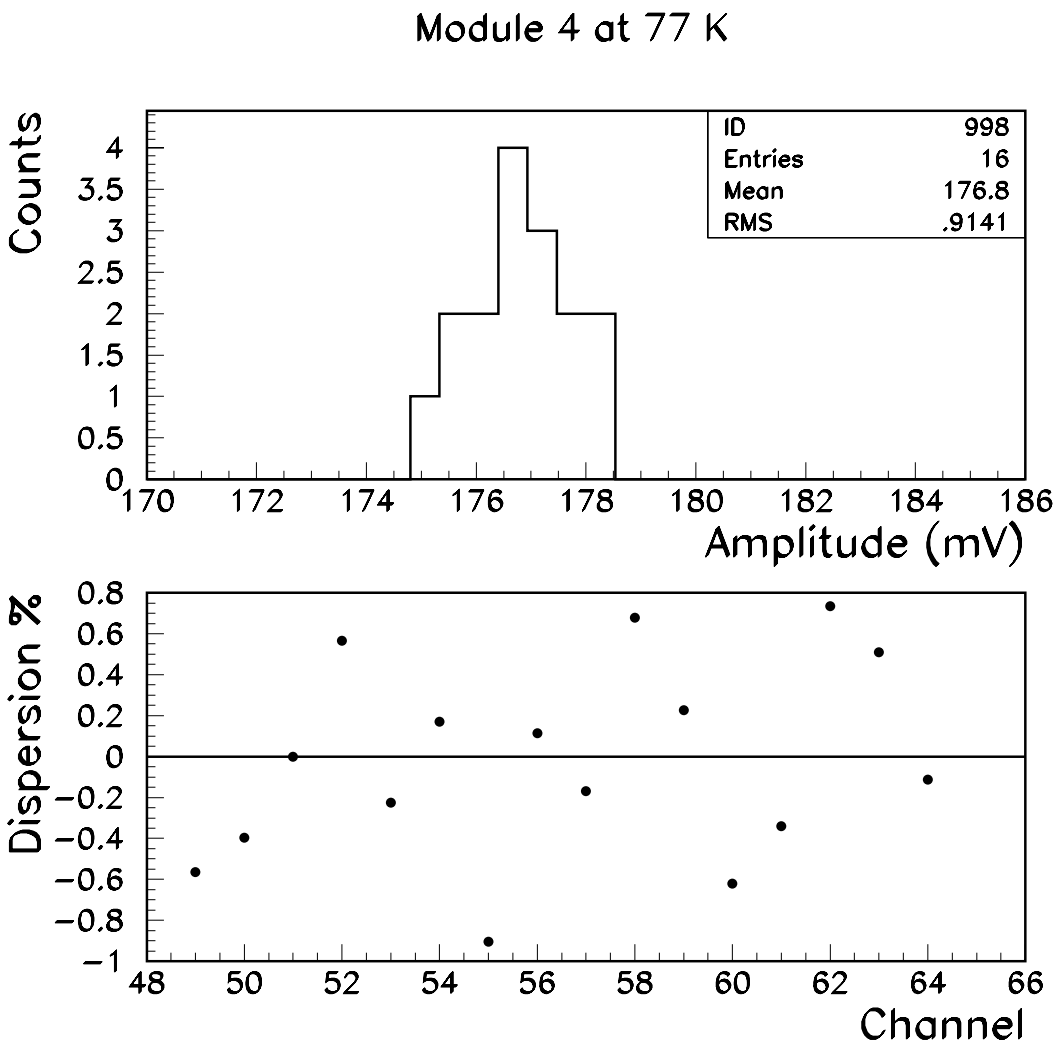

Figure 17: Distribution (upper) and dispersion (lower) around the mean value of the response amplitude when a triangular signal is injected into the calibration circuit.

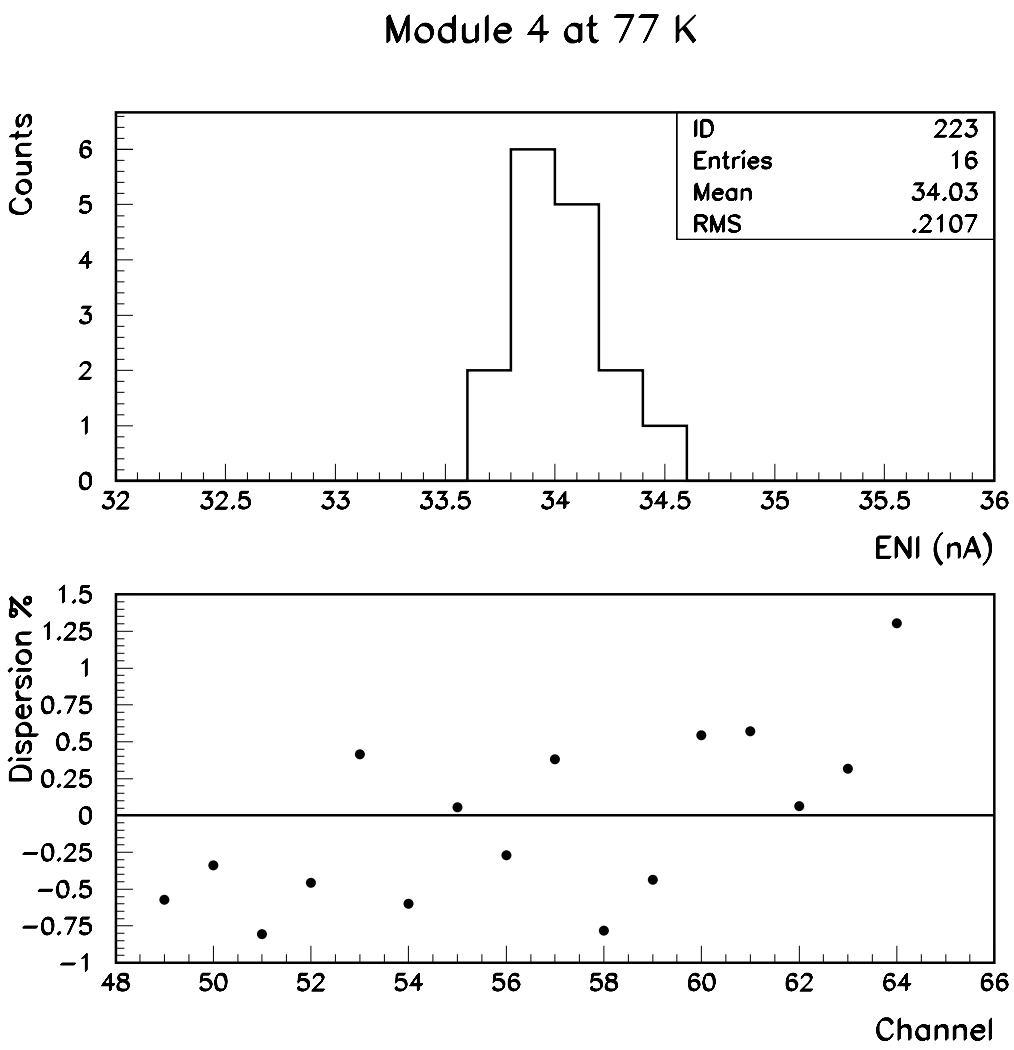

Figure 18: Distribution (upper) and dispersion (lower) around the mean value of the ENI.

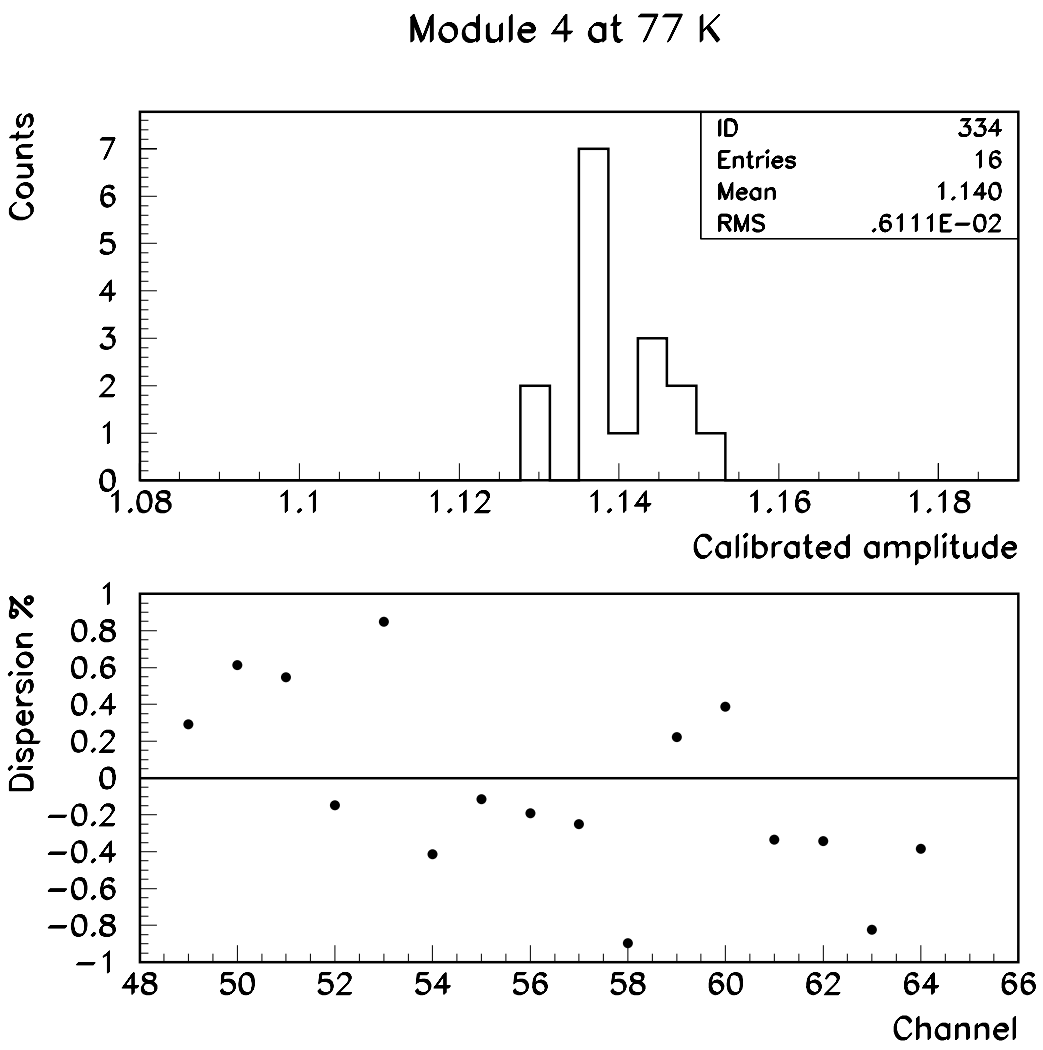

Figure 19: Distribution (upper) and dispersion (lower) around the mean value of the peak-to-peak calibrated amplitude when a sinusoidal signal is injected into the first high voltage bus.

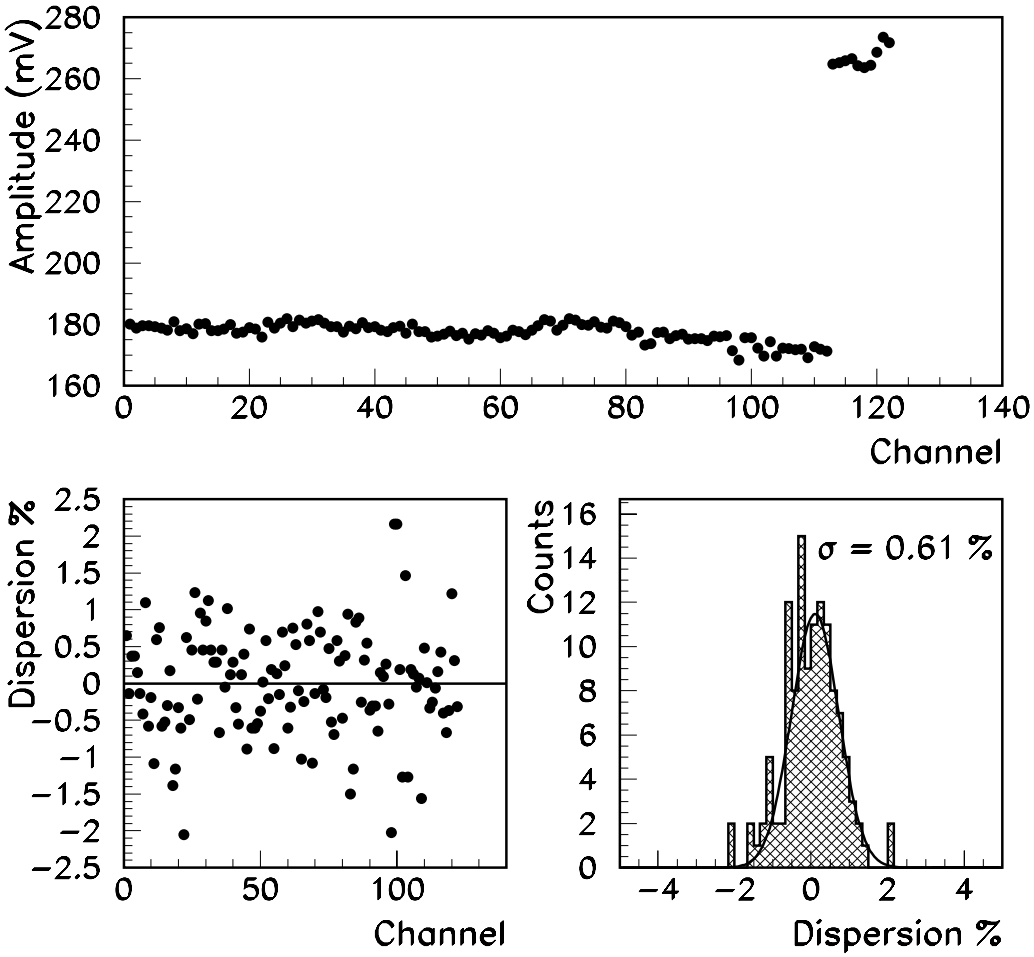

Figure 20: Upper: Response amplitude when test pulses are injected into the calibration circuits of sector 01 at 77 K. The shift observed for the last channels is due to the fact that the injected test pulses are shared into 10 channels instead of 16 in the last MB. Lower left: dispersion around the mean value calculated for each module. Lower right: projection of the previous dispersion.

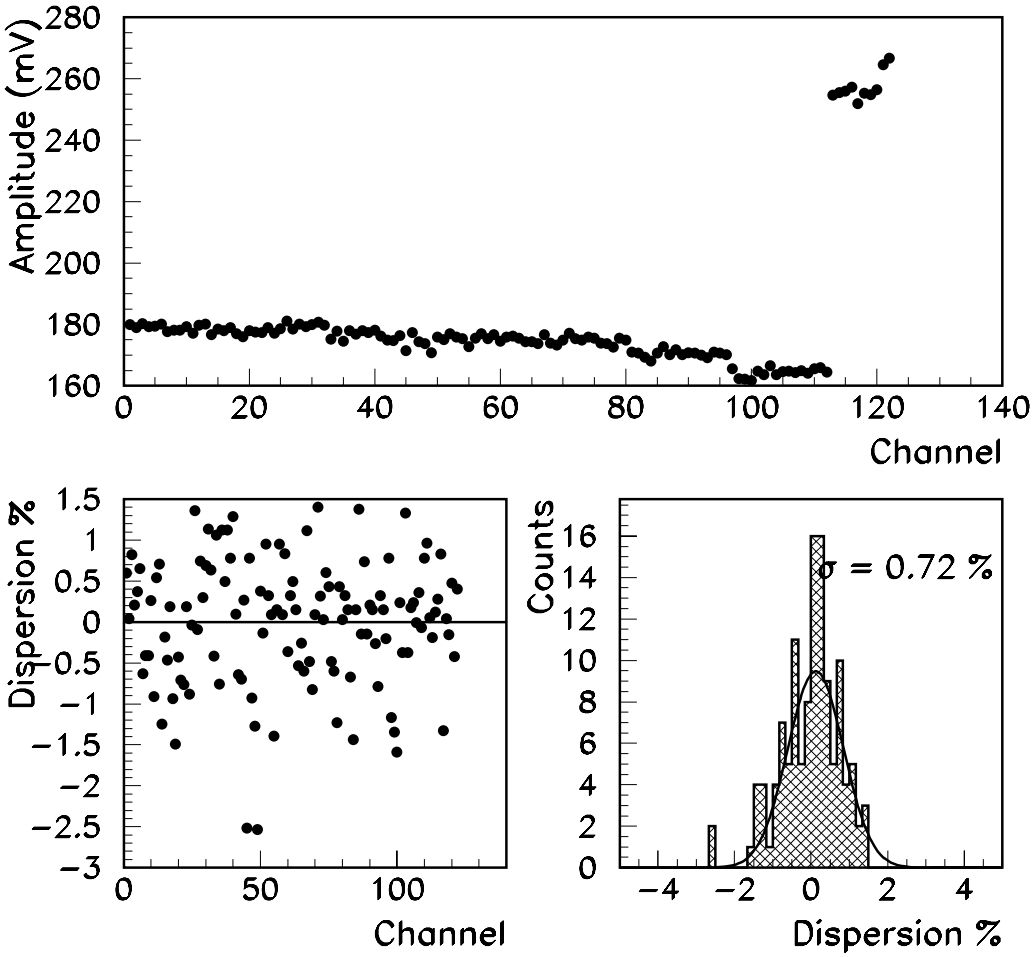

Figure 21: Upper: Response amplitude when test pulses are injected into the calibration circuits of sector 02 at 77 K. The shift observed for the last channels is due to the fact that the injected test pulses are shared into 10 channels instead of 16 in the last MB. Lower left: dispersion around the mean value calculated for each module. Lower right: projection of the previous dispersion.

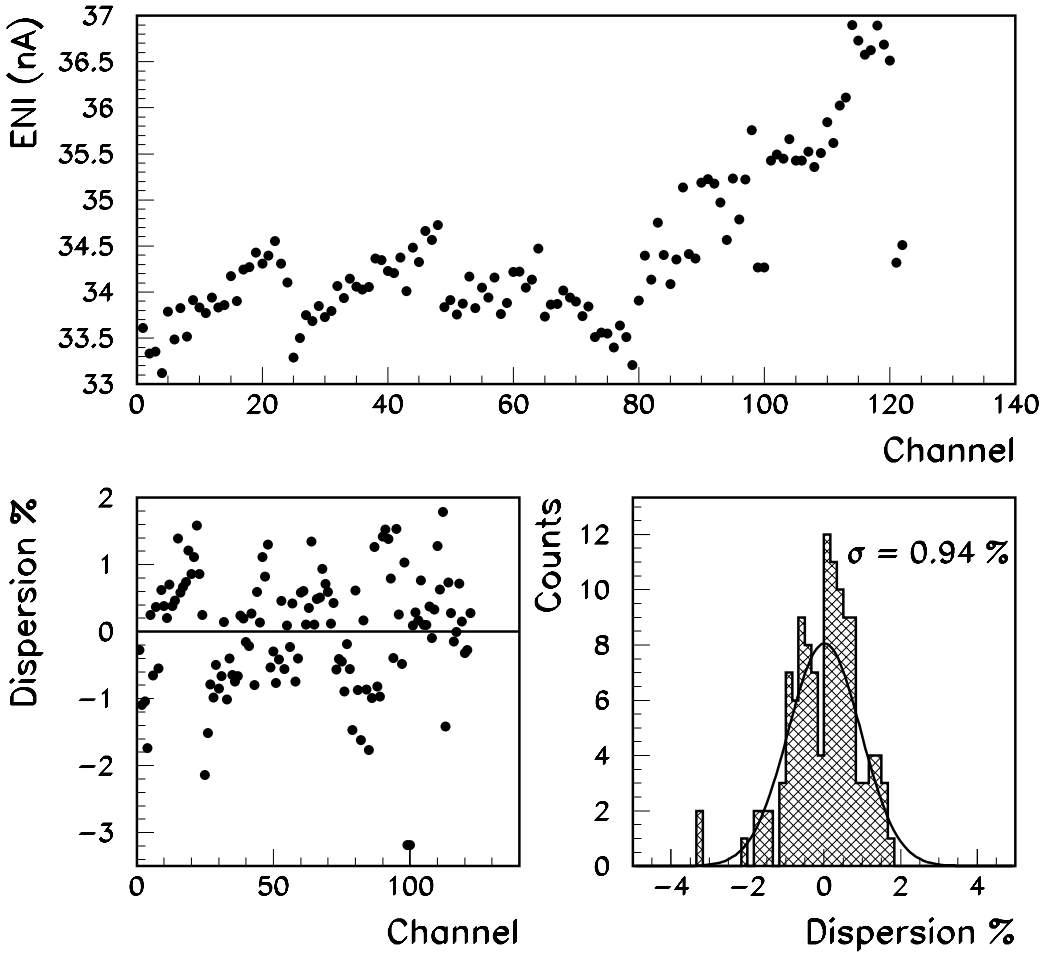

Figure 22: Upper: distribution of the ENI for sector 01 at 77 K. Lower left: dispersion of the ENI around the mean value of each module. Lower right: projection of the previous dispersion.

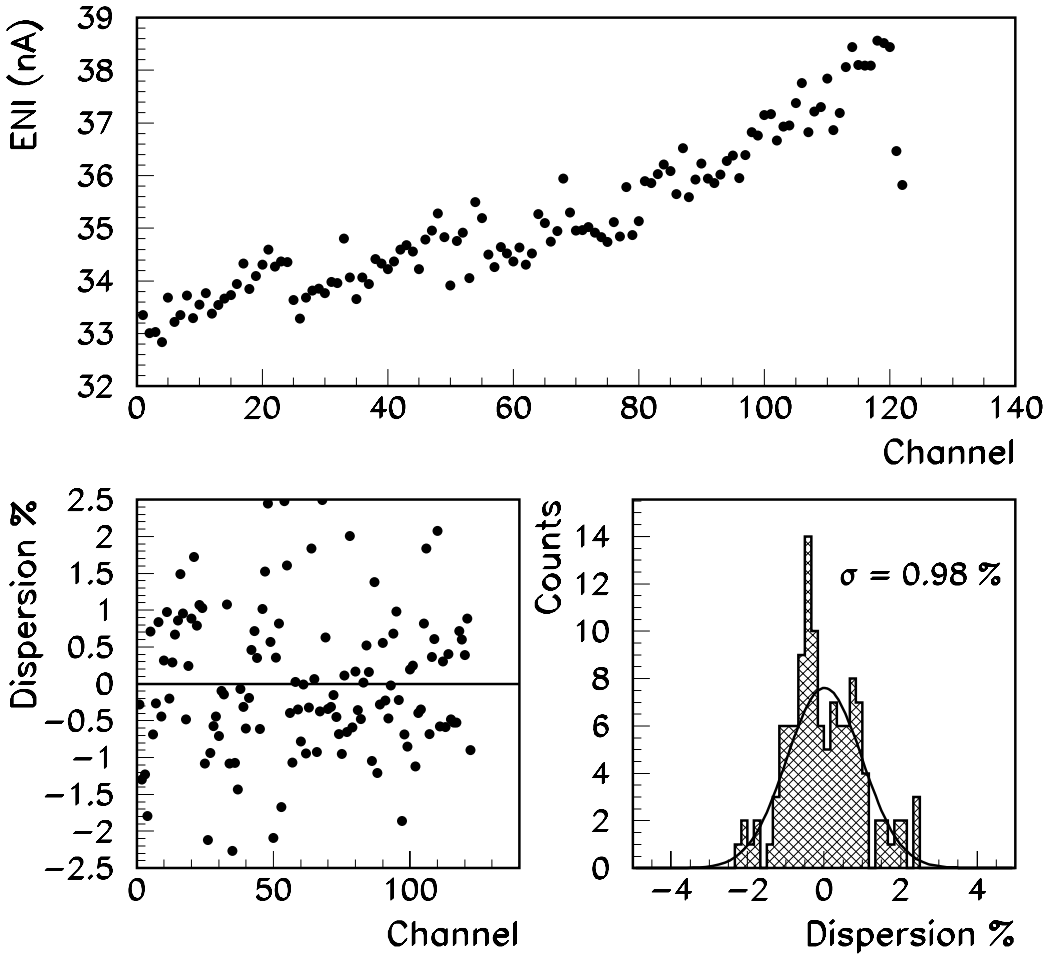

Figure 23: Upper: distribution of the ENI for sector 02 at 77 K. Lower left: dispersion of the ENI around the mean value of each module. Lower right: projection of the previous dispersion.

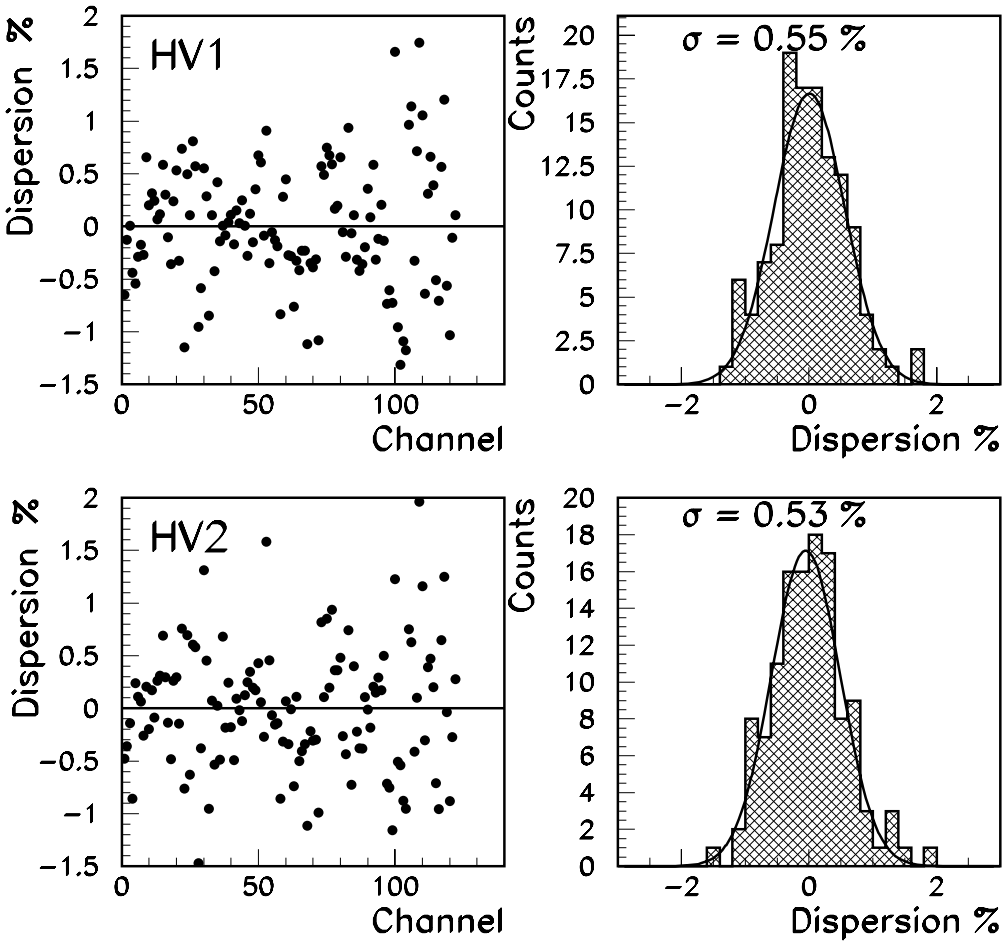

Figure 24: Left: dispersion of the response of sector 01 at 77 K to a sinusoidal signal injected into the HV buses. Right: projection of the previous dispersion around the mean value.

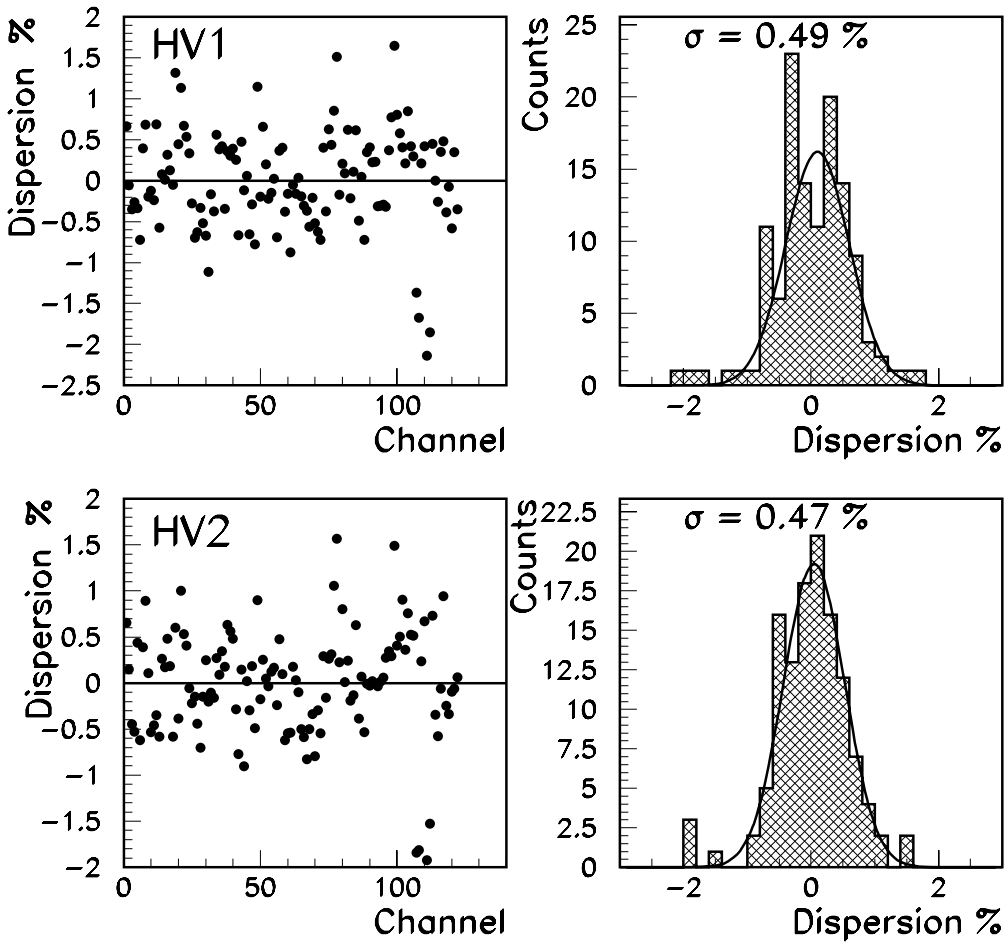

Figure 25: Left: dispersion of the response of the sector 02 at 77 K to a sinusoidal signal injected into the HV buses. Right: projection of the previous dispersion around the mean value.